

Quantitative assessment of computational efficiency of numerical models for surface flow simulation

Yanxia Shen and Chunbo Jiang*

State Key Laboratory of Hydrosience and Engineering, Department of Hydraulic Engineering, Tsinghua University, Beijing 100084, China

*Corresponding author. E-mail: jcb@tsinghua.edu.cn

ABSTRACT

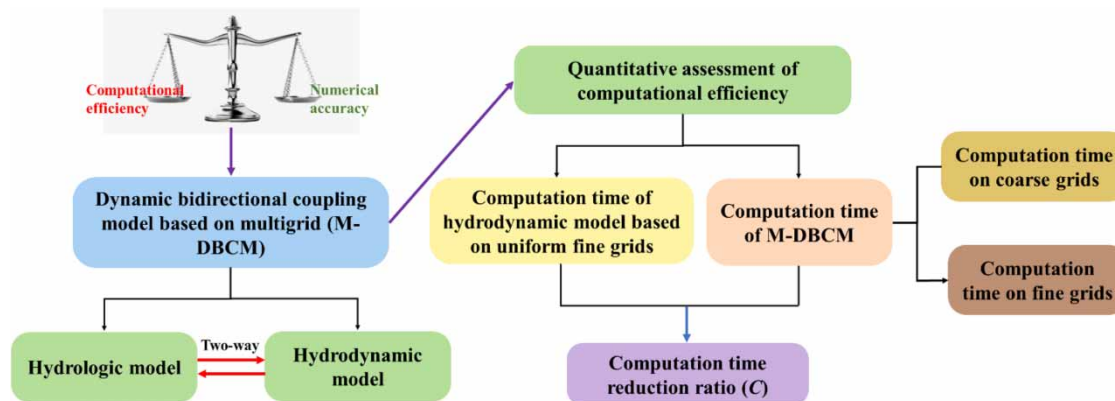
To improve computational efficiency without accuracy losses for surface flow simulation, a dynamic bidirectional coupling model based on multigrid was applied. The flood-prone areas, where the inundation conditions were needed to detail, were discretized using finer grids, while the rest of the domains were assigned coarser grids to reduce computation time. Different time steps were adopted in coarse and fine grids. This paper presented an approach to quantitatively assess the computational efficiency under different domain discretization and grid generation conditions. Three test cases were considered to demonstrate the performance of the applied model. The results showed that the model had high computational efficiency while maintaining satisfactory simulation accuracy. The computational efficiency of the model was not only related to the size ratio of coarse to fine grids, but the area ratio of coarse grids to the entire computational domain. If the area ratio of coarse grids to the computational domain was constant, the computational efficiency improved exponentially with the increasing size ratio. If the size ratio of coarse to fine grids was constant, the computational efficiency improved linearly with the increasing area ratio. The proposed method offers a promising option for quantitatively assessing the computational efficiency of models.

Key words: computational efficiency, dynamic bidirectional coupling model, numerical accuracy, quantitative assessment

HIGHLIGHTS

- A dynamically coupled hydrologic-hydrodynamic model is applied.
- A parameter is proposed to quantitatively assess the computational efficiency.
- The efficiency exponentially improves with the increase of the grid size ratio.
- The efficiency linearly improves with the increase of coarse grids.

GRAPHICAL ABSTRACT



1. INTRODUCTION

Numerical models play a major role in predicting flood processes, e.g., pollutant and sediment transports (Saadatpour *et al.* 2019; Jelti & Boulerhcha 2022). These models are capable of providing accurate solutions, which have received much attention in recent years (Guan *et al.* 2014; Fernández-Pato *et al.* 2020; Li *et al.* 2021). Associated with these numerical models, two main issues normally raised concerns, i.e., numerical accuracy and computational efficiency. Many attempts have been made to improve the numerical accuracy, such as developing a coupling model (Feistl *et al.* 2014; Salheddine *et al.* 2020; Gomes *et al.* 2021), dividing domain with refine grids (Schumann *et al.* 2013, 2014; Li *et al.* 2016; David & Schmalz 2021). These methods increase numerical precision, but are not conducive to improving computing efficiency. For example, if a large domain is divided using fine uniform grids, many computational nodes are involved, which substantially costs more computational resources and time. Therefore, this essentially restricts the application of the numerical model in realistic flood simulations that usually involve large domains.

Several methods are proposed to improve the computational efficiency of numerical models. Schumann *et al.* (2013) and Bates *et al.* (2010) developed a simplified partial inertial model ignoring the dynamics term in full two-dimensional (2D) shallow water equations (SWEs), and the results showed the simplified model can save more computational time compared with the full 2D SWEs. However, since the dynamic terms are not considered, the model cannot reliably reproduce the physical processes and predict the velocity of rapidly varying flows, such as dam breaks.

To further improve computational efficiency, many researchers have optimized the grid resolution during flood simulations, and adaptive mesh refinement (AMR) is the most common method (Hu *et al.* 2018; Ghazizadeh *et al.* 2020). The computational domain was decomposed into coarse grids that were linked with sub-grid sets of various sizes. These dynamically adaptive meshes can adjust grid density in accordance with the domain features or flow conditions, which can be applied for local grid refinement. Liang *et al.* (2015) used the AMR to divide the computational domain, where high-resolution simulation was carried out in areas in which the surface water flow needs to be detailed. The results indicated that complex grid adaptation seems to cost more computation time and resources, although they improve the computational efficiency in comparison with the overall fined grids. In addition to the intricate grid generation techniques, a lot of storage requirements are also needed, which further restrict its applications, especially in larger watersheds. Besides, the mass and momentum conservation may not be ensured at the same time when using a dynamically adaptive grid to divide the computational domain (Bermudez & Ma 1994). It is well known that mass conservation is a critical element to be satisfied in models for practical applications, while momentum conservation influences the numerical stability of models and thereby is important to preserve its robustness.

Static nonuniform grids for surface water flow simulations have received increasing attention in recent years. The flood-prone areas where the inundation conditions are needed to detail are discretized using finer grids, while the rest of the regions are deployed using coarse grids. This method can easily achieve local grid refinement and effectively avoid the troublesome dynamical links between numerical solutions obtained from different grids in AMR. Furthermore, compared with AMR, the static nonuniform grids also have the advantage of a simplified grid generation procedure and may save more computation time. Hou *et al.* (2018) proposed a static nonuniform grid system to identify and refine the crucial regions where a high-resolution grid is essential for accurate surface flow simulation, which can save more computation cost and time than AMR. However, the computational efficiency is limited by the grid sizes, since a 2:1 rule is introduced and no cell is allowed to have a neighbor that is more than twice bigger or smaller. A multigrid dynamic bidirectional coupling model (M-DBCM) based on multi-grids was developed by Shen *et al.* (2021), where different size ratios of coarse to fine grids were used to divide the computational domain. The computational efficiency improved in various degrees based on different size ratios. However, a superficial assessment of computational efficiency was carried out to evaluate the performance of the M-DBCM.

It is also crucial to evaluate the computational efficiency of the numerical model. Hou *et al.* (2018) evaluated the simulation accuracy of the proposed model using the root mean square error, but only the computation time was reported. No further discussion and analysis were adopted on the improvement in computational efficiency. Other researchers, e.g., Shen *et al.* (2021), Yu & Duan (2017), Liu *et al.* (2019) and Jiang *et al.* (2021), have quantitatively assessed the numerical accuracy by comparing the simulation results with a measure or analytical data. Only computational efficiency was reported, but it is lacking in strictly quantitative analysis. At present, the computational efficiency of models is simply assessed by comparing them with the computation time of different algorithms, without further discussing and analyzing the influence factors and improvement degree of computational efficiency. Nevertheless, it is significant to determine the factors influencing

computational efficiency and assess sensitivity of these factors for improving the performance of models. The degree of improvement in computing efficiency is also important to study the performance of the model. The underlying question is how to quantitatively evaluate the computational efficiency of the numerical model and analyze the factors influencing efficiency.

Based on the M-DBCM proposed by our team, this work is devoted to proposing a method to quantitatively evaluate the computational efficiency of models. The remainder of this paper is arranged as follows: the multigrid technique was introduced first; and then the dynamically coupled hydrologic-hydrodynamic model used in this study was detailed; thirdly, an assessment parameter was produced and its derivation process was also described in detail; Section 3 quantitatively demonstrated the computational efficiency of the M-DBCM based on three cases; and Section 4 described the conclusions.

2. METHODS

In this study, a dynamic bidirectional coupled hydrologic-hydrodynamic model proposed by our team based on multigrid is applied. The M-DBCM consists of two components: a hydrologic model that simulates overland flow in the upstream area and a hydrodynamic model that details flood processes in the downstream area vulnerable to floods. For the model setup, multigrid is designed to discretize the computational domain. The Fortran programming language is adopted to apply the coupling model.

2.1. Multigrid generation

The balance between the need of improving resolution in simulating flood processes and computational costs makes it desirable to refine the model grid locally. A structured multigrid system is developed in M-DBCM. The grid system is designed to provide fined grid cells at certain parts of the areas where high-resolution representation is crucial for flood simulation, while the rest of the domain is discretized into coarse cells. The areas where high-resolution representation is crucial can be determined according to topographic data. Generally speaking, low-lying areas, such as rivers and lakes, are vulnerable to floods. Therefore, the parts that require high-resolution representation were marked. And then, refine the marked areas while coarsening the rest of the domain.

A schematic diagram of the multigrid system is presented in Figure 1. Two types of connecting lines are produced, dividing the entire computing area into three parts. The first type is the green line shown in Figure 1, which is used to link coarse and fine grids. The grid size changes suddenly on both sides of this line. The second type, the red line shown in Figure 1, is moving, formed on the fine grids.

The three parts consist of one coarse-grid region and two fine-grid regions. A hydrologic model is applied to simulate the rainfall runoff on coarse-grid regions. The fine grids are divided into two parts, i.e., inundation and noninundation regions. A water depth threshold is used as a simple way for determining these two parts. In a grid cell, if the water depth is higher than the predefined threshold, it is considered an inundation region, where the hydrodynamic model is applied; conversely, if the water depth is lower than the threshold, it is defined as noninundation region, where the hydrologic model is applied. When the rain intensity increases, the inundation regions expand because of the gradual accumulation of surface water volume. The position of inflow discharge positions, flow path and discharge values change subsequently. Therefore, a moving coupling interface (Line-2) is formed between the inundation and noninundation regions. The hydrologic and hydrodynamic models are coupled in a two-way manner, and the coupling boundary is moving and time-dependent.

2.2. The dynamic coupled hydrologic-hydrodynamic model

2.2.1. Hydrologic model

A hydrologic model is used to simulate rainfall runoff, including runoff generation and runoff routing. The hydrologic model consists of a 2D mass balance equation and Manning equations (Bradbrook *et al.* 2004), as follows:

$$\frac{\partial h}{\partial t} + \frac{\partial(hu)}{\partial x} + \frac{\partial(hw)}{\partial y} = q_r \quad (1)$$

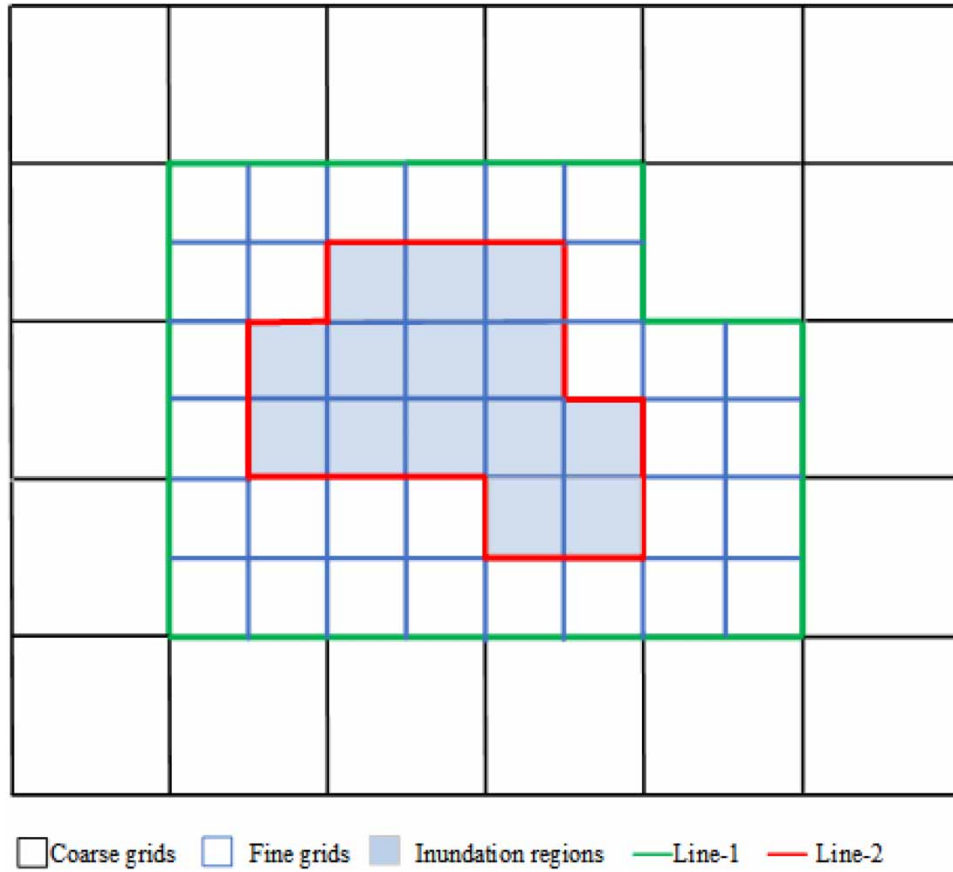


Figure 1 | Schematic diagram of nonuniform grid.

$$q_x = \frac{h^{5/3} S_x^{1/2}}{n_r} \quad (2)$$

$$q_y = \frac{h^{5/3} S_y^{1/2}}{n_r} \quad (3)$$

where h is the water depth (m); u and v are velocities in the x and y directions (m/s); $hu = q_x$ and $hv = q_y$ are the unit discharge in the x and y directions (m^2/s), respectively, which are calculated by Equations (2) and (3); q_r equals to rainfall intensity minus infiltration rate (m/s); S_x and S_y are the water level gradients in the x and y directions, respectively, $S_x = -\partial/\partial x(z + h)$, $S_y = -\partial/\partial y(z + h)$, z is the bottom elevation (m); n_r is Manning's roughness coefficient.

2.2.2. Hydrodynamic model

The 2D SWEs (Toro 2001), consisting of mass and momentum conservation equations, are used as the hydrodynamic model, which can be written as:

$$\frac{\partial h}{\partial t} + \frac{\partial(hu)}{\partial x} + \frac{\partial(hv)}{\partial y} = q_r \quad (4)$$

$$\frac{\partial(hu)}{\partial t} + \frac{\partial(hu^2 + gh^2/2)}{\partial x} + \frac{\partial(huv)}{\partial y} = -gh \frac{\partial z}{\partial x} - \frac{gn^2 |u| \sqrt{u^2 + v^2}}{h^{1/3}} \quad (5)$$

$$\frac{\partial(hv)}{\partial t} + \frac{\partial(huv)}{\partial x} + \frac{\partial(hv^2 + gh^2/2)}{\partial y} = -gh \frac{\partial z}{\partial y} - \frac{gn^2 |v| \sqrt{u^2 + v^2}}{h^{1/3}} \quad (6)$$

where g is gravity acceleration (m/s^2).

2.2.3. The coupling of hydrologic-hydrodynamic model

In fine-grid areas, the dynamically coupled hydrologic-hydrodynamic model is applied to simulate the flooding process. The hydrologic and hydrodynamic models are coupled by a moving coupling interface. The key issue of the model coupling is to develop a reasonable method to determine the fluxes passing through the coupling interface, which should integrate the effect of the current flow state obtained from these two models on both sides of the coupling interface.

An example is provided to explain the change in the position of the coupling boundary and the calculation of fluxes through the coupling boundary, as shown in Figure 2. The local Riemann problem is formed at the coupling boundary. The Harten, Lax, vanLeer and Contact (HLLC) approximate Riemann solver is used to solve the mass and momentum fluxes through the coupling boundary, and a pair of characteristic wave speeds is used to determine which module is used to calculate the fluxes, which are expressed as follows:

$$S_L = u_{i,j} - \sqrt{gh_{i,j}} \quad (7)$$

$$S_R = u_{i+1,j} + \sqrt{gh_{i+1,j}} \quad (8)$$

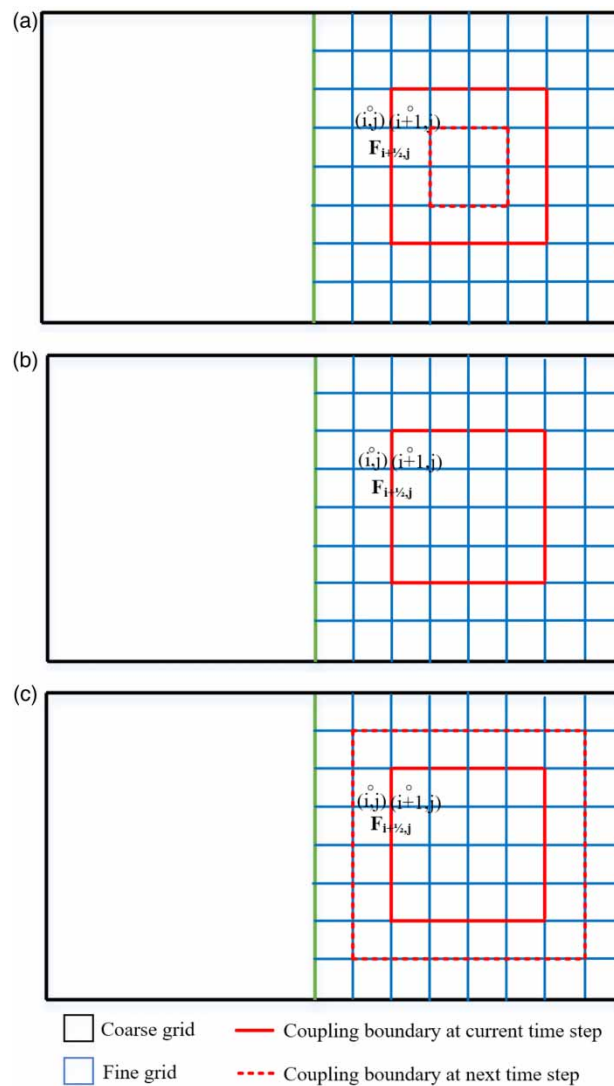


Figure 2 | The coupling boundary of hydrologic and hydrodynamic models: (a) moves from noninundation to inundation regions; (b) remained unchanged and (c) moves from inundation to noninundation regions.

where S_L , S_R are the characteristic wave speeds in noninundation and inundation regions, subscript i, j refers to the grid cell in noninundation regions, while $i + 1, j$ is the grid cell in inundation regions.

If the wave speeds are all positive, that is, $S_R > 0$, $S_L > 0$, the coupling boundary may move from noninundation to inundation regions. The flux calculation through the coupling boundary depends entirely on the information of noninundation regions, and the calculation function can be written as

$$F_{i+1/2,j} = F_L = \begin{bmatrix} hu \\ 0 \end{bmatrix}_{i,j} \quad (9)$$

Based on Equation (9), only the mass conservation through the coupling boundary can be obtained under this situation.

If $S_L < 0 < S_R$, the position of the coupling boundary remains unchanged, as shown in Figure 2(b). The fluxes through the coupling boundary are calculated using both the hydrologic and hydrodynamic models, as shown in Equation (10):

$$F_{i+1/2,j} = f(F_L, F_R) = \frac{S_R F_L - S_L F_R + S_L S_R (U_R - U_L)}{S_R - S_L} \quad (10)$$

$$\text{where } U_L = \begin{bmatrix} h \\ 0 \end{bmatrix}_{i,j}, U_R = \begin{bmatrix} h \\ hu \end{bmatrix}_{i+1,j}, F_L = \begin{bmatrix} hu \\ 0 \end{bmatrix}_{i,j}, F_R = \begin{bmatrix} hu \\ hu^2 + gh^2/2 \end{bmatrix}_{i+1,j}.$$

If $S_L < 0$, $S_R < 0$, the position of the coupling boundary may move from inundation to noninundation regions, as shown in Figure 2(c). The flux calculation through the coupling boundary depends only on the information of inundation regions, as follows:

$$F_{i+1/2,j} = F_R = \begin{bmatrix} hu \\ hu^2 + gh^2/2 \end{bmatrix}_{i+1,j} \quad (11)$$

Based on Equations (10) and (11), both the mass and momentum conservation through the coupling boundary can be obtained. The flow and discharge of information at inundation and noninundation regions can also affect each other.

In the presented dynamic bidirectional coupling approach, overland flow can be discharged from the inundation regions to noninundation regions and the effects owing to the overflow of the floodplain and backwater effects at confluences are also considered.

A time explicit scheme is used to solve the hydrologic and hydrodynamic models. The time step is constrained by the Courant–Friedrichs–Lewy condition (Delis & Nikolos 2013) and is a dynamic adjustment according to the velocity and water depth in the computational domain. In the proposed M-DBCM, different time steps are used in coarse and fine grids. The time step used in fine grids is calculated as follows:

$$\Delta t_1 = \min \left\{ C_r \min \left(\frac{\min(\Delta x_1)}{\max(|u_1| + \sqrt{gh_1})}, \frac{\min(\Delta y_1)}{\max(|v_1| + \sqrt{gh_1})} \right) \right\} \quad (12)$$

where C_r is a constant to maintain format stability, $1/2 \leq C_r < 1$; Δx_1 and Δy_1 are the length and width of the fine grid (m), respectively; u_1 and v_1 are the flow velocity on the fine grids along the x and y directions (m/s), respectively; and h_1 is the water depth on the fine grids (m).

The time step of the coarse grids (Δt_2) was determined based on that of the fine grids. If the size of the coarse grid was n times that of the fine grid, the time step of the coarse grid was determined to be $\Delta t_2 = n\Delta t_1$.

2.3. The assessment of computational efficiency

In M-DBCM, the computational domain is divided into coarse and fine grids, as shown in Figure 1. The area of the whole computational domain can be expressed as:

$$A = A_1 + A_2, A_2 > A_1 \quad (13)$$

where A is the area of the entire computational domain; A_1 is the area of fine-grid regions; A_2 is the area of coarse-grid regions.

If the entire watershed is divided by fine uniform grids, and only the 2D hydrodynamic model (hereinafter referred to as HM2D) is used to simulate the flood processes. The computation time of HM2D based on the fine uniform grids is:

$$t_0 = \alpha \cdot \frac{A}{\Delta x_1^2} \cdot \frac{T_{end}}{\Delta t_1} \quad (14)$$

where t_0 is the computation time of HM2D (s); Δx_1 is the size of fine grids (m), T_{end} is the simulation time (s); Δt_1 is the time step on fine grids (s); α is the runtime of hydrodynamic model at one calculation node (s), which is depended on computer power and numerical model complexity.

As for the M-DBCM, the computation time on fine and coarse grids can be calculated by Equations (15) and (16), respectively, as follows:

$$t_1 = \alpha \cdot \frac{A_1}{\Delta x_1^2} \cdot \frac{T_{end}}{\Delta t_1} \quad (15)$$

$$t_2 = \beta \cdot \frac{A - A_1}{\Delta x_2^2} \cdot \frac{T_{end}}{\Delta t_2} \quad (16)$$

where, t_1 , t_2 are the computation time on fine and coarse grids, respectively (s); Δx_2 is the size of coarse grids (m); Δt_2 is the time step on coarse grids (s); β is the runtime of hydrologic model at one calculation node (s), which is dependent on computer power and numerical model complexity. Since the hydrodynamic model is expressed by a nonlinear hyperbolic equation and hydrologic model is expressed by a linear equation, the calculation of the hydrodynamic model is more complicated than that of the hydrologic model, which results in $\beta/\alpha < 1$.

Except for the computation time of hydrologic and hydrodynamic models, the time required in other ways (i.e., the coupling of hydrologic and hydrodynamic model, the variables interchange between coarse and fine grids) can be expressed as $t_3 = \alpha_0 t_1$. Therefore, the computation time of M-DBCM is $t_1 + t_2 + t_3 = (1 + \alpha_0)t_1 + t_2$.

The computational efficiency of M-DBCM is accordingly assessed using the following equation:

$$C = \frac{(1 + \alpha_0)t_1 + t_2}{t_0} = \frac{(1 + \alpha_0)\alpha \frac{A_1}{\Delta x_1^2} \left(\frac{T_{end}}{\Delta t_1}\right) + \beta \frac{A - A_1}{\Delta x_2^2} \left(\frac{T_{end}}{\Delta t_2}\right)}{\alpha \frac{A}{\Delta x_1^2} \left(\frac{T_{end}}{\Delta t_1}\right)} \quad (17)$$

where C is an assessment parameter indicating the computation time reduction ratio, which is used to evaluate the computational efficiency of M-DBCM. A smaller C value means higher computational efficiency.

Compared with the AMR where intricate grid adaptation and interpolation may cost much computation time, the grid generation technique used in M-DBCM can save more computation time. The time required in the coupling of hydrologic-hydrodynamic model and variables interchange between coarse and fine grids is far less than that required in the hydrodynamic model, that is $\alpha_0 \ll 1$. For convenience, the α_0 is set to 0 in this study. And Equation (17) may be rewritten as:

$$C = \frac{\alpha \frac{A_1}{\Delta x_1^2} \left(\frac{T_{end}}{\Delta t_1}\right) + \beta \frac{A - A_1}{\Delta x_2^2} \left(\frac{T_{end}}{\Delta t_2}\right)}{\alpha \frac{A}{\Delta x_1^2} \left(\frac{T_{end}}{\Delta t_1}\right)} \quad (18)$$

The time step ratio of coarse grids to fine grids is equal to the size ratio of coarse grids to fine grids, as follows:

$$\frac{\Delta t_2}{\Delta t_1} = \frac{\Delta x_2}{\Delta x_1} \quad (19)$$

Based on Equation (19), Equation (18) can be rewritten as:

$$C = \frac{A_1}{A} + \frac{\beta}{\alpha} \left(\frac{\Delta x_1}{\Delta x_2} \right)^3 \frac{A - A_1}{A} \quad (20)$$

By defining $n = \frac{A_2}{A}$ ($0 < n \leq 1$), $\Delta t_2 = k\Delta t_1$ ($k \geq 1$), Equation (20) becomes

$$C = (1 - n) + \frac{\beta}{\alpha k^3} n \quad (21)$$

From Equation (21), the computational efficiency of M-DBCM is not only related to the size ratio of coarse to fine grids, but the area ratio of coarse grids to the entire domain. If the area of coarse-grid regions is much greater than that of the fine-grid regions, that is, $n \rightarrow 1$, the assessment parameter becomes $C \propto \beta/\alpha 1/k^3$. It is indicated that the computational efficiency of M-DBCM exponentially improves with the increase of the size ratio. If the size of coarse grids is much more than that of fine grids, that is, $k \rightarrow \infty$, the assessment parameter becomes $C \propto (1 - n)$. It is stated that the computational efficiency of M-DBCM improves linearly with the increasing of the area ratio of the coarse grids to the entire domain.

3. CASE STUDY

The performance of the proposed M-DBCM is demonstrated by applying it to three cases. The results are compared with those obtained from the model that has similar numerical schemes but on uniform fine grids, referred to as DBCM in the following sections. Besides, the HM2D on fine uniform grids is also applied to the same cases to compare with the proposed model.

3.1. Rainfall runoff over a slope plane

In this case, a rainfall runoff on a constant slope (Kim *et al.* 2012) is designed to evaluate the performance of M-DBCM. The sketch of the case is shown in Figure A.1 in the Supplementary Material. The length of the plane is 182.88 m. A Manning's coefficient of $0.025 \text{ s/m}^{1/3}$ is recommended. The bed slope is 0.016. The constant rainfall intensity is 50.8 mm/h. The rainfall duration is 1,800s and the total simulation time is performed for 3,600 s. Different cases with various grid size ratios were designed to evaluate the performance of the M-DBCM, as listed in Table B.1 in the Supplementary Material. In M-DBCM, the size of fine grids is 1.83 m while the rest of the domain is coarsened to levels higher, as presented in Figure A.2 in the Supplementary Material. Fine uniform grids with a resolution of 1.83 m are also adopted for comparative simulations.

The hydrographs simulated by the M-DBCM based on different grid size ratios at the watershed outlet were compared with the analytical solution, as shown in Figure 3. It is observed that the hydrographs obtained from different cases were consistent with the analytical solution, whether in discharge rising or receding limbs, which indicated that the M-DBCM exhibited satisfactory simulation accuracy. However, in peak discharge, the hydrographs obtained from the different cases were slightly underpredicted, but the error was acceptable.

The total computational time of different cases on a desktop computer with an Intel i7-11700K CPU and 64G RAM was determined, presented in Table 1. Since uniform fine grids were applied in case00 and case01, the computation time of both cases was higher than that of others. Case01 cost more computational time compared with case00 due to the solution of 2D SWEs in the whole region. Most areas were discretized into coarse grids, whereas only a small part of regions was divided into fine grids in case12, case15 and case10; the number of cells was much lower than that of case00 and case01. As a result, the computation time of M-DBCM based on nonuniform grids was lower than that of the others.

The computational efficiency evaluation parameter C of different cases is shown in Figure 4. Lower C values mean higher computational efficiency. If the size ratio of coarse to fine grids is constant, C values decreased linearly with the development of n . Higher n means larger coarse-grid regions. It is well known that the simulations on coarse grids involve few computational nodes and substantially cost less computation time. From this figure, if n is constant, C values decreased with the increasing size ratio of coarse to fine grids. The size of fine grids is the same ($1.83 \text{ m} \times 1.83 \text{ m}$) in case12, case15 and case10, but the size of coarse grids is different in these cases. The sizes of coarse grids are twice, 5 times and 10 times that of fine grids in case12, case15 and case10, respectively. Therefore, the computational grids of these three cases

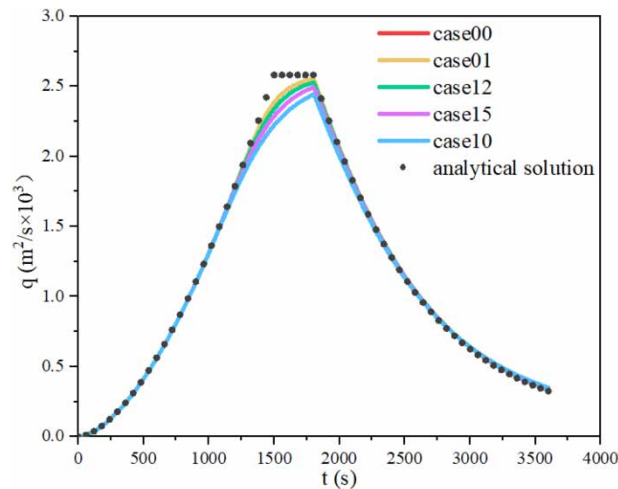


Figure 3 | Comparison of hydrographs obtained from different cases with analytical solution ($n = 0.5$).

Table 1 | Runtimes of different cases in Section 3.1

N	Cases	Number of grids	Runtimes (s)
–	case00	1,000	94.422
–	case01	1,000	99.812
0.3	case12	820	83.719
	case15	784	79.281
	case10	772	77.344
0.5	case12	655	65.704
	case15	544	59.609
	case10	527	58.775
0.7	case12	505	52.875
	case15	352	45.797
	case10	329	44.484

ranked from more to less are: case12 > case15 > case10. Fewer computational grids required less time for calculation. The computational efficiency could be further improved with the increasing size ratio of the coarse grid to the fine grid.

The C values of case12, case15 and case10 were 0.59, 0.56 and 0.55, respectively, when $n = 0.3$; while the C values of case12, case15 and case10 were 0.36, 0.28 and 0.25, respectively, when $n = 0.7$. It is observed that the variation degree of C values was different when n varied. The total computation time is mainly dependent on that of fine grids since fine-grid regions are large when n is small.

3.2. Rainfall runoff over a plane with variable slope and roughness

In this case, a sloping plan measuring $500 \text{ m} \times 400 \text{ m}$ was designed, with slopes $S_{ox} = 0.02 + 0.0000149x$ and $S_{oy} = 0.05 + 0.0000116y$ along the x and y directions, respectively (Jaber & Mohtar 2003), presented in Figure A.3 in the Supplementary Material. The Manning's coefficient is equal to $n = \sqrt{n_x^2 + n_y^2}$, where $n_x = 0.1 - 0.0000168x$ and $n_y = 0.1 - 0.0000168y$. The rainfall intensity is given by a symmetric triangular hyetograph $r = r(t)$ with $r(0) = r(200 \text{ min}) = 0$ and $r(100 \text{ min}) = 0.8 \times 10^{-5} \text{ m/s}$. The simulations are run for 14,400 s. Except for a transmissive boundary at the watershed outlet, the other boundaries were reflective. Different cases, as shown in Table B.2 in the Supplementary Material, were developed to simulate the rainfall runoff. In M-DBCM, the size of fine grids was $1 \text{ m} \times 1 \text{ m}$ while the rest of the domain was coarsened to levels higher, as presented in Figure A.4 in the Supplementary Material. Fine uniform grids with a resolution of $1 \text{ m} \times 1 \text{ m}$ were also adopted for comparative simulations, as case00 and case01 shown in Table B.2.

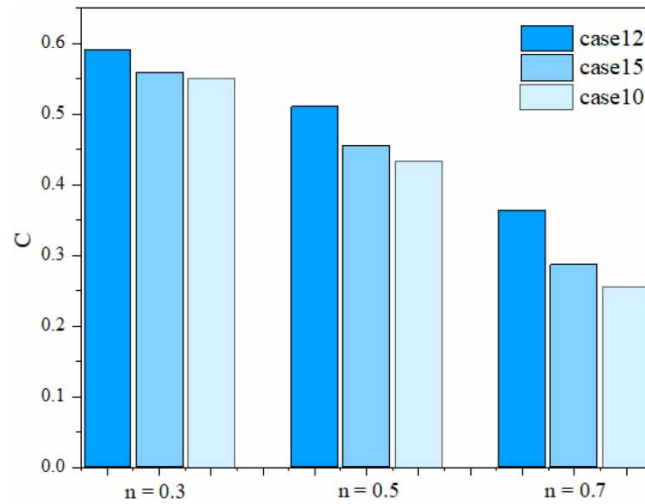


Figure 4 | C values of different cases in Section 3.1.

The integrated flood modeling system (IFMS) (Wu *et al.* 2018; Yang *et al.* 2021) and a model developed by Jaber & Mohtar (2003) were used to simulate the rainfall runoff process under the same conditions, which were used to assess the performance of the M-DBCM. The hydrographs obtained from different models are shown in Figure 5. Really fine grids were used to divide the computational domain to obtain more accurate results in the model developed by Jaber & Mohtar (2003). Therefore, it can be considered that the results obtained from Jaber & Mohtar (2003) was equivalent to the approximate analytical solution. The hydrographs showed good agreement, indicating that the simulation accuracy of the M-DBCM were satisfactory. The peak discharge and receding limb simulated by IFMS were slightly under-predict discharge. The 2D SWEs were solved to simulate the flooding process in the whole regions in IFMS, while the M-DBCM converted from a hydrodynamic model to a hydrologic model when the water depth was below the threshold. When the M-DBCM converted from hydrodynamic model to hydrologic model, the approach to calculate the velocity is also changed accordingly, then the discharge difference between the IFMS and M-DBCM appeared. The outlet flow was slightly larger, but later slightly smaller in M-DBCM, assuring that the overall mass was conserved.

The runtimes of different cases were reported, as presented in Table 2. A comparison was first made between the fine uniform grids and nonuniform grids to check the difference between these two mesh representations. The computation time of

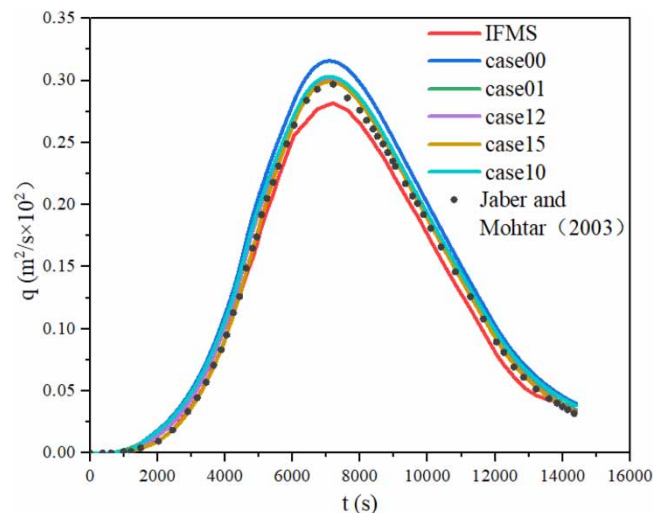


Figure 5 | Comparison of hydrographs obtained from different cases ($n = 0.5$).

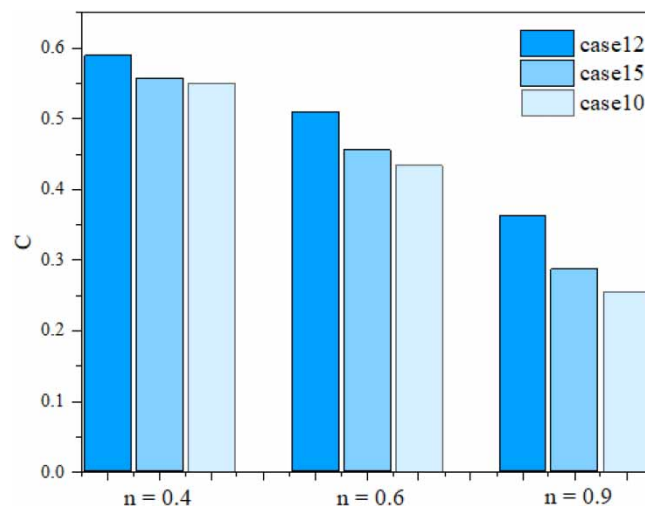
Table 2 | Runtimes of different cases on section 3.2

n	Cases	Number of grids	Runtimes (s)
–	case00	200,000	6,404.828
–	case01	200,000	7,871.844
0.4	case12	142,090	4,651.515
	case15	128,088	4,404.905
	case10	127,463	4,328.813
0.6	case12	115,127	4,025.687
	case15	92,122	3,594.938
	case10	91,779	3,415.014
0.9	case12	66,062	2,863.735
	case15	29,405	2,259.016
	case10	25,670	2,009.016

the case00 and case11 was higher than that of others. A total of 200,000 grids were generated based on fine uniform grids. Most of the areas were discretized into coarse grids, and only a small part of the region was divided into fine grids on a non-uniform grids system; the calculation grid number was much lower than that of case00 and case01. Consequently, the computation time of fine uniform grids was much larger than that of nonuniform grids. Furthermore, case01 cost more computational time and resources compared with other cases, due to the solution of the 2D SWEs in the whole region.

The C values were calculated to assess the computational efficiency of M-DBCM, as shown in Figure 6. When $n = 0.4$, the C values ranged from 0.5 to 0.6, which indicated that the computational efficiency improved by about 40% based on the multi-grids. The C decreased linearly with the increase of n . When $n = 0.9$, the coarse grid regions accounted for 90% of the total watershed. The C values ranged between 0.25 and 0.40, indicating that the computational efficiency improved by about 70% when the computational domain meshed with multi-grids. When n is constant, C values decreased with the increasing of the size ratio. The size of fine grids is the same in all the cases. In case12, the size of coarse grid is twice that of the fine grid, while the size of the coarse grid is 5 times and 10 times that of the fine grids in case15 and case10, respectively. The number of grid cells ranked from more to less is as follows: case12 > case15 > case10. Therefore, case12 cost more computation time compared with case15 and case10. The computation time decreased with the increase in the size of the coarse grids, resulting in diminishing C values.

In addition, an interesting phenomenon was observed in this figure. When $n = 0.4$, C values changed slightly in case12, case15 and case10. But C values of different cases changed a lot with the increase of n . When $n = 0.9$, C values of case12,

**Figure 6** | C values of the different cases in Section 3.2.

case15 and case10 were 0.36, 0.29 and 0.25, respectively. When n is small, the coarse-grid regions accounted for a small proportion of the entire computational domain, and the number of fine grids is larger. The total runtimes mainly depended on the computation time of fine grids. Consequently, closer C values were produced in different cases when n is small. The proportion of coarse grids in the computational domain increased with the increase of n . When $n = 0.9$, the number of grids varied greatly in different cases. Therefore, the computation time of different cases also has great differences. It was concluded that the area ratio of the coarse-grid regions to the entire domain had a great influence on computational efficiency.

3.3. Flood simulation in a natural watershed

The Goodwin Creek watershed is located in Panola County, Mississippi, USA, which covers an area of 21.3 km². The overall terrain gradually decreased from northeast to southwest, which is consistent with the trend of the main channel, and the elevation ranged from 71 to 128 m. The computational basin and bed elevations are shown in Figure A.5 in the Supplementary Material. Land use in this watershed was divided into four classes including forest, water, cultivated and pasture, and their Manning coefficients were 0.05, 0.01, 0.03 and 0.04, respectively (Sánchez 2002). The infiltration coefficients of different soil types were determined according to Blackmarr (1995).

The rainfall duration was 4.8 h. The simulations were performed for 12 h. Different cases with various grid resolutions were developed to verify the computational efficiency and numerical accuracy of M-DBCM, as listed in Table B.3 in the Supplementary Material. In M-DBCM, the rivers were covered by fine-grid cells of 10 m × 10 m while the rest of the domain was coarsened to levels higher, presented in Figure A.6 in the Supplementary Material. Fine uniform grids with a resolution of 10 m were also adopted for comparative simulations.

The hydrographs at the watershed outlet obtained from different cases were shown in Figure 7. A closer match has been produced at different models, which indicated that the results were encouraging and the overall trend was well captured. Satisfactory agreement was also achieved between the hydrographs obtained from fine uniform grids and the ones computed by M-DBCM, which indicated that the simulation accuracy was not reduced due to the division of different grid sizes in M-DBCM.

In terms of computational efficiency, the total execution time for simulating surface flow based on different cases was determined, presented in Table 3. Uniform fine grids were used to divide the computing zones in case00 and case01, where the calculation grid number was 207,198. Consequently, both cases had high computational burden and cost more computation time. In case01, as the 2D SWEs were calculated in all regions, which required a large volume of computational time and

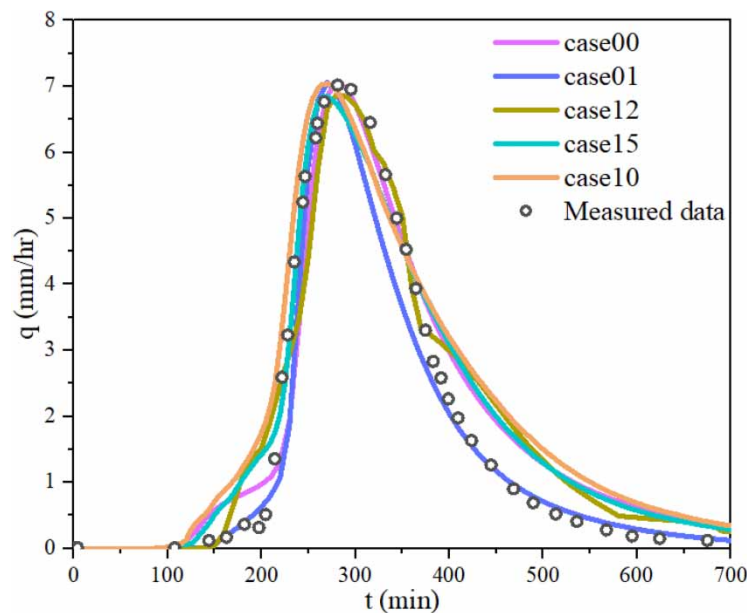


Figure 7 | Comparison of hydrographs obtained from different cases ($n = 0.7$).

Table 3 | Runtimes of different cases on section 3.3

n	cases	Number of grids	runtimes (h)
–	case00	207,198	40.13
–	case01	207,198	42.91
0.5	case12	151,063	22.65
	case15	102,560	22.08
	case10	93,640	21.80
0.7	case12	104,555	21.82
	case15	80,109	20.69
	case10	76,114	19.71

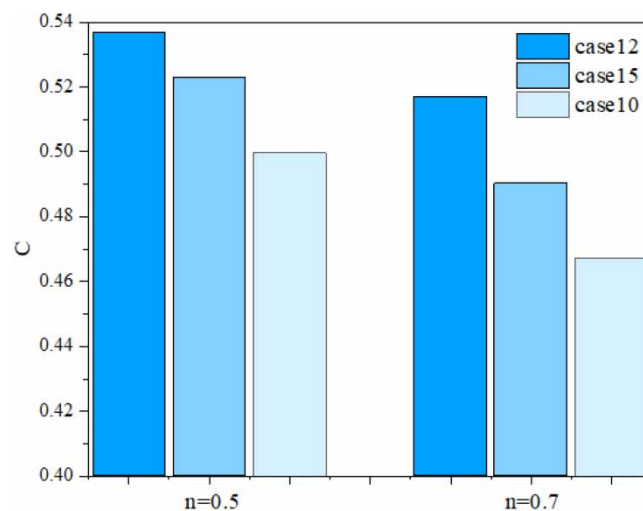
resources, the simulation time was higher than that of case00. In the multigrid system, the computation grid number was much lower than that of case00, which can save more computation time.

To quantitatively analyze the computational efficiency of the M-DBCM, C values of different cases were calculated, as shown in Figure 8, when $n = 0.5$, that were 0.528, 0.515 and 0.508, respectively. In contrast, when $n = 0.7$, C values of case12, case15 and case10 were 0.509, 0.482 and 0.459, respectively. C values decreased with the increase of n , which indicated that the area ratio of coarse grids to the entire computational domain had a great influence on the computational efficiency. Larger coarse-grid regions mean less computation time since there were few calculation grids. If n is constant, C values decreased with the increase of the size ratio of coarse to fine grids. There were fewer calculation grids in the larger size ratio, which required less time for calculation; therefore, the computational efficiency can be improved.

However, it is noted that C values of different cases changed slightly in the condition where $n = 0.5$, compared with that in the condition where $n = 0.7$. It was demonstrated that the computational efficiency was affected by the area ratio of coarse grids to the entire computational domain. In the condition where $n = 0.7$, the coarse-grid regions were much more than fine-grid regions. The total runtimes mainly depended on the computation time on coarse grids. The calculation grid number decreased a lot with the increase in the size ratio of coarse grids to fine grids. The computation time was consequently reduced. When $n = 0.5$, the total runtimes mainly depended on the computation time on fine grids. High-resolution simulations on fine grids inevitably involved a large number of computational nodes and substantially increased computational cost.

4. CONCLUSIONS

A dynamic bidirectional coupling model with a nonuniform grid was applied in this study to improve computational efficiency and meanwhile preserve simulation accuracy, and an assessment parameter was developed to quantitatively assess

**Figure 8** | C values of different cases in Section 3.3.

the computational efficiency of models. The regions where high-resolution representation was needed in a computational domain were divided into fine grids, while the rest of the regions were deployed using coarse grids to reduce the computational burden. The hydrologic model was applied to the coarse grid regions, while on the fine grids, the hydrologic and hydrodynamic models were coupled in a two-way manner to ensure mass and momentum conservation. The computation time on coarse and fine grids was analyzed, respectively. Based on this, a parameter for assessing computational efficiency was proposed.

The performance of M-DBCM was validated against three test cases. Numerical results were compared with those predicted on fine uniform grids. The M-DBCM was demonstrated to be able to effectively simulate the flow process and ensure reliable simulations. While producing numerical results of similar accuracy, the M-DBCM saved much computation time compared with the DBCM or HM2D on fine grids. The computational efficiency was quantitatively evaluated based on an assessment parameter. Lower C values mean higher computational efficiency. C values varied in different cases. Three important conclusions were obtained based on the C values. Firstly, if the area ratio of coarse grids to the entire domain was constant, only the size ratio of coarse to fine grids had influence on the computational efficiency; the computation time decreased dramatically with the increase of the size ratio. Secondly, if the size ratio of the coarse to fine grids was constant, only the proportion of coarse grids in the entire computational domain had an effect on the computational efficiency; the computation time decreased linearly with the increasing of the area ratio of coarse grids to the entire computational domain. Lastly, if there were fewer coarse-grid regions, C values decreased slightly with the increase of the size ratio of coarse to fine grids because the total runtimes mainly depended on computation time on fine grids under this condition.

The proposed M-DBCM is able to accurately and efficiently reproduce the flooding process and therefore has the potential for a wide range of practical applications. Unstructured grids would be used to divide the computational domain since they provide great flexibility in comforting complex domain geometries. The GPU may also be used to accelerate the computation time.

ACKNOWLEDGEMENTS

This study was supported by the National Science Foundation of China (No. 52179068) and the Key Laboratory of Hydroscience and Engineering (No. 2021-KY-04). The authors thank the anonymous reviewers for their valuable comments.

DATA AVAILABILITY STATEMENT

All relevant data are included in the paper or its Supplementary Information.

CONFLICT OF INTEREST

The authors declare there is no conflict.

REFERENCES

- Bates, P. D., Horritt, M. S. & Fewtrell, T. J. 2010 A simple inertial formulation of the shallow water equations for efficient two-dimensional flood inundation modelling. *Journal of Hydrology* **387** (1–2), 33–45. <http://doi.org/10.1016/J.JHYDROL.2010.03.027>.
- Bermudez, A. & Ma, E. V. 1994 Upwind methods for hyperbolic conservation laws with source terms. *Computers & Fluids* **23** (8), 1049–1071. [https://doi.org/10.1016/0045-7930\(94\)90004-3](https://doi.org/10.1016/0045-7930(94)90004-3).
- Blackmarr, W. 1995 *Documentation of Hydrologic, Geomorphic, and Sediment Transport Measurements on the Goodwin Creek Experimental Watershed, Northern Mississippi, for the Period 1982–1993*. Technical Report for United States Department of Agriculture, Oxford, MS, USA, October.
- Bradbrook, K. F., Lane, S. N., Waller, S. G. & Bates, P. D. 2004 Two-dimensional diffusion wave modelling of flood inundation using a simplified channel representation. *International Journal of River Basin Management* **3** (2), 211–223. <http://doi.org/10.1080/15715124.2004.9635233>.
- David, A. & Schmalz, B. 2021 A systematic analysis of the interaction between rain-on-grid-simulations and spatial resolution in 2D hydrodynamic modeling. *Water* **13** (17), 2346. <http://doi.org/10.3390/w13172346>.
- Delis, A. & Nikolos, I. 2013 A novel multidimensional solution reconstruction and edge-based limiting procedure for unstructured cell-centered finite volumes with application to shallow water dynamics. *International Journal for Numerical Methods in Fluids* **71**, 584–633. <http://doi.org/10.1002/flid.3674>.
- Feistl, T., Bebi, P., Dreier, L., Hanewinkel, M. & Bartelt, P. 2014 A coupling of hydrologic and hydraulic models appropriate for the fast floods of the Gardon river basin (France). *Natural Hazards & Earth System Sciences* **14** (11), 2899–2920. <http://doi.org/10.5194/nhess-14-2899-2014>.

- Fernández-Pato, J., Martínez-Aranda, S., Morales-Hernández, M. & García-Navarro, P. 2020 Analysis of the performance of different culvert boundary conditions in 2D shallow flow models. *Journal of Hydroinformatics* **22** (5), 1093–1121. <http://doi.org/10.2166/hydro.2020.025>.
- Ghazizadeh, M. A., Mohammadian, A. & Kurganov, A. 2020 An adaptive well-balanced positivity preserving central-upwind scheme on quadtree grids for shallow water equations. *Computers & Fluids* **208**, 104633. <http://doi.org/10.1016/j.compfluid.2020.104633>.
- Gomes, M. M. D., Verçosa, L. F. D. & Cirilo, J. A. 2021 Hydrologic models coupled with 2D hydrodynamic model for high-resolution urban flood simulation. *Natural Hazards* **108**, 3121–3157. <http://doi.org/10.1007/s11069-021-04817-3>.
- Guan, M., Wright, N. G. & Wright, N. G. 2014 2D process-based morphodynamic model for flooding by noncohesive dyke breach. *Journal of Hydraulic Engineering* 44–51. [http://doi.org/10.1061/\(ASCE\)HY.1943-7900.0000861](http://doi.org/10.1061/(ASCE)HY.1943-7900.0000861).
- Hou, J., Wang, R., Liang, Q., Li, Z., Huang, M. S. & Hinkelmann, R. 2018 Efficient surface water flow simulation on static cartesian grid with local refinement according to key topographic features. *Computers & Fluids* **176**, 117–134. <http://doi.org/10.1016/j.compfluid.2018.03.024>.
- Hu, R., Fang, F., Salinas, P. & Pain, C. C. 2018 Unstructured mesh adaptivity for urban flooding modelling. *Journal of Hydrology* **560**, 354–363. <http://doi.org/10.1016/j.jhydrol.2018.02.078>.
- Jaber, F. H. & Mohtar, R. H. 2003 Stability and accuracy of two-dimensional kinematic wave overland flow modeling. *Advances in Water Resources* **26** (11), 1189–1198. [http://doi.org/10.1016/S0309-1708\(03\)00102-7](http://doi.org/10.1016/S0309-1708(03)00102-7).
- Jelti, S. & Boulterhcha, M. 2022 Numerical modeling of two-dimensional non-capacity model for sediment transport by an unstructured finite volume method with a new discretization of the source term. *Mathematics and Computers in Simulation* **197**, 253–276. <http://doi.org/10.1016/j.matcom.2022.02.012>.
- Jiang, C., Zhou, Q., Yu, W., Yang, C. & Lin, B. 2021 A dynamic bidirectional coupled surface flow model for flood inundation simulation. *Natural Hazards and Earth System Sciences* **21** (2), 497–515. <http://doi.org/10.5194/nhes-21-497-2021>.
- Kim, J., Warnock, A., Ivanov, V. Y. & Katopodes, N. D. 2012 Coupled modeling of hydrologic and hydrodynamic processes including overland and channel flow. *Advances in Water Resources* **37**, 104–126. <http://doi.org/10.1016/j.advwatres.2011.11.009>.
- Li, D., Wang, X., Xie, Y., Chen, J., Tian, Y., Chen, W. & Cai, X. 2016 A multi-level and modular model for simulating the urban flooding and its application to Tianjin city. *Natural Hazards* **82** (3), 1947–1965. <http://doi.org/10.1007/s11069-016-2279-z>.
- Li, Z., Chen, M. Y., Gao, S., Luo, X. Y., Gourley, J. J., Kirstetter, P., Yang, T. T., Kolar, R., McGovern, A., Wen, Y. X., Rao, B., Yami, T. & Hong, Y. 2021 CREST-IMAP v1.0: a fully coupled hydrologic-hydraulic modeling framework dedicated to flood inundation mapping and prediction. *Environmental Modelling and Software* **141** (1), 105051. <http://doi.org/10.1016/j.envsoft.2021.105051>.
- Liang, Q., Hou, J. & Amouzgar, R. 2015 Simulation of tsunami propagation using adaptive cartesian grids. *Coastal Engineering Journal* **57** (4), 1550016.1–1550016.30. <https://doi.org/10.1142/S0578563415500163>.
- Liu, Z., Zhang, H. & Liang, Q. 2019 A coupled hydrological and hydrodynamic model for flood simulation. *Nordic Hydrology* **50** (1–2), 589–606. <http://doi.org/10.2166/nh.2018.090>.
- Saadatpour, M., Afshar, A. & Khoshkam, H. 2019 Multi-objective multi-pollutant waste load allocation model for rivers using coupled archived simulated annealing algorithm with QUAL2KW. *Journal of Hydroinformatics* **21** (3), 397–410. <http://doi.org/10.2166/hydro.2019.056>.
- Salheddine, M., André, P. & Mahmoud, H. 2020 A coupled 1-D/2-D model for simulating river sediment transport and bed evolution. *Journal of Hydroinformatics* **22** (5). <http://doi.org/10.2166/hydro.2020.020>.
- Sánchez, R. R. 2002 *GIS-Based Upland Erosion Modeling, Geovisualization and Grid Size Effects on Erosion Simulations with CASC2D-SED*. PhD Thesis, Colorado State University, Fort Collins, CO, USA.
- Schumann, G. J. P., Neal, J. C., Voisin, N., Andreadis, K. M., Pappenberger, F., Phanthuwongpakdee, N., Hall, A. C. & Bates, P. D. 2013 A first large-scale flood inundation forecasting model. *Water Resource Research* **49** (10), 6248–6257. <http://doi.org/10.1002/wrcr.20521>.
- Schumann, J. P., Andreadis, K. M. & Bates, P. D. 2014 Downscaling coarse grid hydrodynamic model simulations over large domains. *Journal of Hydrology* **508**, 289–298. <http://doi.org/10.1016/j.jhydrol.2013.08.051>.
- Shen, Y., Jiang, C., Zhou, Q., Zhu, D. & Zhang, D. 2021 A multigrid dynamic bidirectional coupled surface flow routing model for flood simulation. *Water* **13**, 3454. <https://doi.org/10.3390/w13233454>.
- Toro, E. F. 2001 *Shock-Capturing Methods for Free-Surface Shallow Flows*. John Wiley. <http://doi.org/10.1086/116188>.
- Wu, J., Yang, R. & Song, J. 2018 Effectiveness of low-impact development for urban inundation risk mitigation under different scenarios: a case study in Shenzhen, China. *Natural Hazards & Earth System Sciences* **18**, 2525–2536. <http://doi.org/10.5194/nhess-2017-402>.
- Yang, B., Ma, J., Huang, G. & Cao, D. 2021 Development and application of 3D visualization platform for flood evolution in Le'an river basin of Wuyuan. *IOP Conference Series Earth and Environmental Science* **638** (1), 012053. (9 pp). <http://doi.org/10.1088/1755-1315/638/1/012053>.
- Yu, C. & Duan, J. G. 2017 Simulation of surface runoff using hydrodynamic model. *Journal of Hydrologic Engineering (ASCE)* **22** (6), 04017006. [http://doi.org/10.1061/\(ASCE\)HE.1943-5584.0001497](http://doi.org/10.1061/(ASCE)HE.1943-5584.0001497).

First received 30 August 2022; accepted in revised form 25 February 2023. Available online 9 March 2023